FLIGHT MECHANICAL ANALYSIS OF A VERY FLEXIBLE HIGH-ALTITUDE PLATFORM UNDER UNCERTAINTY CONSIDERATIONS

Yasim J. Hasan[1], Nicolas Fezans[1] & Arne Voß[2]

[1]Institute of Flight Systems, German Aerospace Center (DLR), Lilienthalplatz 7, 38108 Braunschweig, Germany
[2]Institute of Aeroelasticity, German Aerospace Center (DLR), Bunsenstraße 10, 37073 Göttingen, Germany

Abstract

The German Aerospace Center (DLR) is currently developing a fixed-wing solar-powered high-altitude platform which is supposed to be stationed in the stratosphere for 30 days carrying payload of up to 5 kg. The project also involves a comprehensive low-altitude flight test campaign. This paper deals with a flight mechanical investigation of the high-altitude platform considering uncertainties. The aircraft has a wing span of 27 m and a total mass of around 140 kg. Therefore, it has a delicate structure and is highly flexible. In order to increase the probability of a successful first flight test campaign, several analyses dealing with the aircraft's flight dynamics and controllability have already been performed using the flexible flight dynamics model implemented within the project. However, in practice, it is to be expected that the actual aircraft's flight mechanical properties will differ from those of the model due to modelling assumptions, limitations of the analysis methods used and due to manufacturing inaccuracies. Therefore, it must be ensured that the aircraft still has acceptable flight mechanic properties if the actual behaviour deviates in an unfavourable way. In a first step, weight and balance and aerodynamic parameters are varied sequentially in order to determine their respective influences. The results show that model uncertainties tend to have the largest effect at lower altitudes and for eigenmodes that are already close to the real axis. In case of the phugoid mode, a variation of the mass and the main wing lift curve slope have an opposing effect at low altitudes and low airspeeds compared to high altitudes and high airspeeds. For the Dutch roll it is observed that at low altitudes, where this eigenmode is strongly damped, coupling derivatives between roll and yaw have the strongest influence. At higher altitudes, however, the mode is weakly damped and it is more dependent on roll damping, weathercock stability and static roll stability. In a second step, all parameters are varied randomly at the same time. In this investigation, no critical case is identified.

Keywords: high-altitude platform, flight mechanics, structural dynamics, uncertainties

1. Introduction

The German Aerospace Center (DLR) is currently developing a complete high-altitude platform (HAP) system in the context of the project *HAP*. The HAP system includes the fixed-wing HAP aircraft itself, the flight control system and the complete operational concept, the ground segment, the flight termination system and two instruments used as payload with a mass of up to 5 kg each. The aircraft is designed to perform Earth observation missions carrying either a high-definition camera or a synthetic aperture radar. The aircraft development process has just passed the detail design phase. Within the further project term, the manufacturing and a comprehensive flight test campaign will follow. The flight permission for the flight test is obtained based on the specific operational risk assessment (SORA) [1] developed by the Joint Authorities of Rulemaking on Unmanned Systems (JARUS) and endorsed by the European Aviation Safety Agency (EASA) [2].

Flying in the lower stratosphere, HAPs are located above commercial air traffic and thus bring benefits with respect to several use cases, which usually lie in the field of satellite applications. Compared

to satellites, the trajectories of HAPs can be chosen more freely while a satellite's position and its associated passing times are dependent on its orbit. Thus, combining the advantages of satellites with those of air vehicles, HAPs represent excellent candidates for general Earth observation missions [3], surveillance in case of humanitarian crises or natural catastrophes, support for agricultural tasks, or health monitoring and telecommunications [4].

For these reasons, research work on HAPs has increased significantly in recent years with several projects dealing with HAPs of different types [5]. Some of the most prominent HAP-related programmes are the NASA ERAST programme [6] producing a great number of aircraft, including the Helios aircraft which holds the current altitude record among HAPs of 96,863 feet [7], the Solar Impulse programme [8], which realised a fully solar-powered manned flight around the world, covering a distance of around 26,718 miles in 2016 [9] and the Airbus Zephyr programme [10] featuring the Zephyr S which recently broke its own endurance record among HAPs of nearly 26 days in 2018 [11] by a 64 days continuous flight performed from June to August 2022 [12].

The BAE Systems PHASA-35 [13] or the UAVOS ApusDuo [14] are other prominent examples of aircraft that also already performed successful flights. However, current programmes are usually part of commercial projects, whose primary aim is to create business or military use cases. Therefore, detailed scientific results and analyses of HAP aicraft are rarely published. Hence, the primary aim of the DLR project *HAP* is to obtain, generate, and publish knowledge about such aircraft rather than to compete with the HAP aircraft already developed by industrial companies.

However, while there are a few HAP aircraft that have performed successful flights on the one side, there have been numerous mishaps that involve HAP aircraft on the other side [12, 15, 16, 17, 18]. Several factors make the design and operation of HAP aircraft a very challenging task. For fixed-wing aircraft, the goal of high endurance requires a very low weight and a very high aspect ratio to realise high aerodynamic efficiency. This leads to a high structural flexibility. Furthermore, the operating speeds are very low with the allowable speed band being very narrow. As a consequence, these aircraft are very susceptible to wind and take-off and landing are critical with respect to a loss of aircraft.

In order to increase the probability of a successful flight test campaign in the context of the project *HAP*, a careful and thorough investigation of the aircraft's flight physics is thus indispensable. In fact, detailed flight mechanic investigations have already been performed for an earlier version of the aircraft [19], allowable wind conditions for different operating tasks have been determined based on pilot-in-the-loop simulations [20], and the landing capabilities have been considered carefully, both using a landing controller [21] and based on pilot-in-the-loop simulations [22].

However, in all these investigations, only the nominal configuration, as determined based on aerodynamic and structural aeroelastic design analyses, was investigated. In practice, however, the actual aircraft's flight characteristics will most likely differ from those of the flight dynamic model. This is both due to modelling assumptions (e.g., a Vortex Lattice Method was used to calculate the aircraft baseline aerodynamics and linear models were used for the calculation of the aeroelastic parameters) and due to manufacturing inaccuracies. Therefore, it must be ensured that the actual aircraft still has acceptable flight mechanical properties. In case of flight control clearance, bounded uncertainties are usually applied to different parameters in such a way that the worst case is obtained followed by an assessment on whether the controller still performs adequately [23].

Since the aircraft is supposed to be piloted remotely, it needs to be investigated whether uncertainties have an adverse effect to the aircraft's handling characteristics. While a determination of the respective worst-case combinations of uncertainties with respect to flight dynamics is also planned for future work, the work presented in this paper focuses on the effect of single uncertainties by solely varying chosen weight and balance and aerodynamic parameters. This is crucial to understand the effect different parameters have on the aircraft's flight dynamics. This is particularly true since previous investigations have shown that the aircraft's eigenmodes differ largely from those of conventional fixed-wing aircraft [19]. The results can then be used to motivate further investigations aiming at reducing the uncertainty level of the parameters which most impact the HAP aircraft behavior. This could involve more thorough investigations by using more sophisticated methods or by ensuring that the manufacturing process will precisely match the desired properties. As a result, the respective

uncertainty with respect to this parameter could then be reduced within the consecutive worst-case assessment.
Hence, this paper deals with a sensitivity analysis of the effect of different parameters on the DLR HAP aircraft's open-loop dynamics. Section 2 briefly presents the investigated aircraft, and section 3 presents the flight dynamic model and the approach used to model the structural dynamics. Section 4 outlines the varied parameters and their variation range and shows the process of how the analysis is followed. Section 5 provides the results with respect to the aircraft's eigenmodes. It presents the nominal eigenmodes, shows the sensitivity analysis and finally shows the effect of parallel parameter variation. Section 6 concludes the paper and section 7 gives a short outlook.

2. The DLR HAP Aircraft

This section presents the DLR HAP aircraft. A sketch of the aircraft is depicted in Figure 1. The vehicle is an ultralight aircraft with a high aspect ratio and outer wing sections with 12° dihedral. The aircraft nose section contains a compartment used to stow the payload. The aircraft is equipped with two propeller engines and has two ailerons, an all moving horizontal stabiliser and a rudder. The aircraft has a total mass of around 140 kg, a wing span of 27 m and a wing area of 36 m^2.

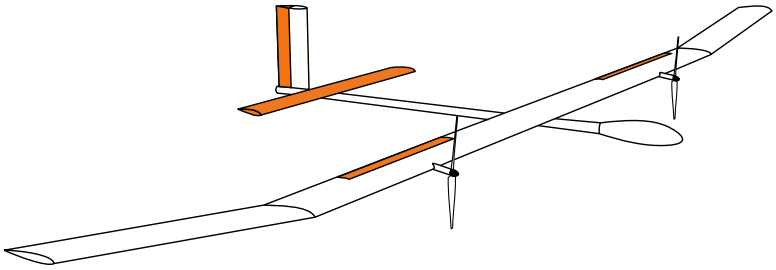

Figure 1 – Sketch of the DLR HAP aircraft

The aircraft's flight envelope is defined by four characteristic airspeeds, which are mainly based on the aeroelastic design speeds as described in [24]. These airspeeds define an outer and an inner envelope. The outer envelope must not be left at any time, because serious damage to the aircraft structure or entering an uncontrollable flight condition would be very likely. This outer envelope is defined by:

- **Stalling speed** V_S (6.5 m/s at sea level): The airspeed shall never fall below this speed (while attempting to sustain its weight) because otherwise stall occurs.
- **Never-exceed speed** V_{NE} (14.5 m/s at sea level): This airspeed shall never be exceeded, otherwise structural damages might occur.

In addition, an inner envelope is defined, which is called the operation envelope. During nominal flight, excluding take-off and landing, the airspeed should not leave the operation envelope. Nevertheless, externally provoked excursions, e.g., due to gusts, are acceptable. However, whenever this happens, a primary concern is reentering the operation envelope. The associated airspeeds are:

- **Minimum operating speed** $V_{O,min}$ (9.1 m/s at sea level): This is the lower limit of the operation envelope.
- **Maximum operating speed** $V_{O,max}$ (11.0 m/s at sea level): This is the upper limit of the operation envelope and thus should not be exceeded deliberately.

At higher altitudes the respective true airspeeds scale according to density such that the equivalent airspeeds remain constant. It should however be noted that at very high altitudes the stalling speed slightly increases while the minimum operating speed slightly decreases due to Reynolds number effects, leading to a smaller safety margin. Figure 2 shows the respective true airspeeds for all aforementioned speeds. Furthermore, it depicts the design manoeuvring speed V_A and the design cruise speed V_C, which $V_{O,min}$ and $V_{O,max}$ are deviated from. V_x is an intermediate speed between V_C and V_{NE} and $V_{L,min}$ and $V_{L,max}$ are the respective minimum and maximum allowable landing speeds.

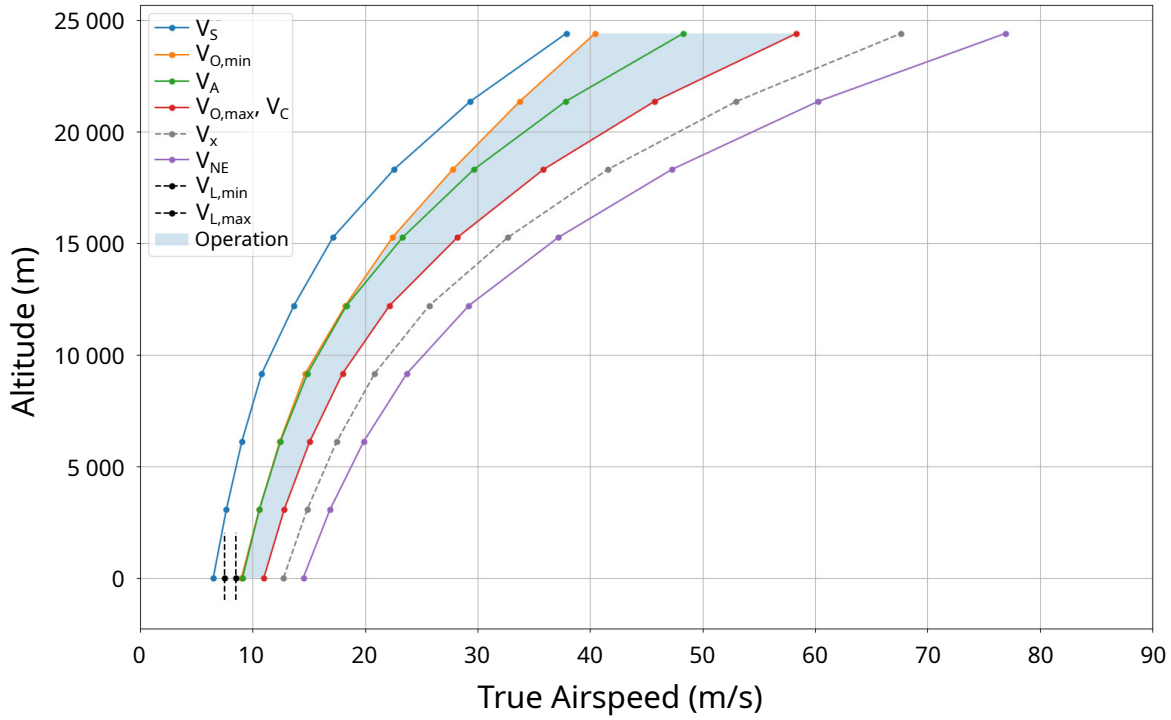

Figure 2 – Design speeds of the DLR HAP aircraft

3. Flight Dynamics Model

The flight dynamics model used within this work is an extension of the 6-degrees-of-freedom-model used and described within earlier works [19, 20]. This earlier model only included flexibility in a quasistatic form. In comparison, the current model used in this work additionally includes the structural dynamics based on the approach proposed by Waszak and Schmidt [25]. The rigid-body equations of motion are thus extended by forces and moments due to the structural dynamics (denoted with the index "Flex"):

$$\begin{aligned} \dot{\vec{V}}_K &= -\vec{\Omega}_K \times \vec{V}_K + \frac{1}{m}\left(\vec{R}_{Prop} + \vec{R}_{Grav} + \vec{R}_{Aero} + \vec{R}_{Flex}\right) \\ \dot{\vec{\Omega}}_K &= \underline{\underline{I}}^{-1}\left(-\vec{\Omega}_K \times (\underline{\underline{I}}\Omega_K) + \vec{Q}_{Prop} + \vec{Q}_{Aero} + \vec{Q}_{Flex}\right) \end{aligned} \tag{1}$$

In the model used here, the aerodynamic forces and moments $\vec{R}_{Aero}$ and $\vec{Q}_{Aero}$ are determined based on a derivative approach. The influences of quasistatic deformation of the aircraft are included in such a way that the aerodynamic derivatives are given for the deformed aircraft at different characteristic airspeeds and for intermediate airspeeds, interpolation is performed. As an example, the equation for the aerodynamic rolling moment then reads (for the complete equations please confer [19, 20]):

$$C_l = C_{l\beta}(V_{EAS}) \cdot \beta + C_{lp}(V_{EAS}) \cdot p^* + C_{lr}(V_{EAS}) \cdot r^* + C_{l\xi}(V_{EAS}) \cdot \hat{\xi} \cdot k_{\xi,eff}(V_{EAS}) + C_{l\zeta}(V_{EAS}) \cdot \zeta \cdot k_{\zeta,eff}, \tag{2}$$

where $k_{\xi,eff}$ is the aileron effectivity due to flexibility and $k_{\zeta,eff}$ is the respective rudder effectivity. For the calculation of the forces and moments $\vec{R}_{Flex}$ and $\vec{Q}_{Flex}$ due to the structural dynamics in equation (1) it must now be respected that the influences due to the quasistatic deformation are already included in the equations of motion via the aerodynamic forces and moments. Therefore, only the deviation from the respective 1g-steady-state flight, matching with the flight shapes for which the derivatives are given, are used to calculate $\vec{R}_{Flex}$ and $\vec{Q}_{Flex}$:

$$\frac{1}{m} \cdot \vec{R}_{Flex} = \begin{bmatrix} \sum_i^{N_{modes}} \dot{u}_{\eta_i} \Delta\eta_i + \sum_i^{N_{modes}} \dot{u}_{\dot{\eta}_i} \Delta\dot{\eta}_i \\ \sum_i^{N_{modes}} \dot{v}_{\eta_i} \Delta\eta_i + \sum_i^{N_{modes}} \dot{v}_{\dot{\eta}_i} \Delta\dot{\eta}_i \\ \sum_i^{N_{modes}} \dot{w}_{\eta_i} \Delta\eta_i + \sum_i^{N_{modes}} \dot{w}_{\dot{\eta}_i} \Delta\dot{\eta}_i \end{bmatrix} \qquad \underline{\underline{I}}^{-1} \cdot \vec{Q}_{Flex} = \begin{bmatrix} \sum_i^{N_{modes}} \dot{p}_{\eta_i} \Delta\eta_i + \sum_i^{N_{modes}} \dot{p}_{\dot{\eta}_i} \Delta\dot{\eta}_i \\ \sum_i^{N_{modes}} \dot{q}_{\eta_i} \Delta\eta_i + \sum_i^{N_{modes}} \dot{q}_{\dot{\eta}_i} \Delta\dot{\eta}_i \\ \sum_i^{N_{modes}} \dot{r}_{\eta_i} \Delta\eta_i + \sum_i^{N_{modes}} \dot{r}_{\dot{\eta}_i} \Delta\dot{\eta}_i \end{bmatrix} \tag{3}$$

Note that, in contrast to [25], no force coefficients are used but the structural dynamic model described in section 3.1 is linearised at different flight points, directly yielding for the rigid-body accelerations due to flexible deformations and rates ($\dot{u}_{\eta_i}$, $\dot{u}_{\dot{\eta}_i}$, etc.). As these are dependent on the flight shapes and altitude, interpolation needs to be performed for them as well:

$$\begin{aligned} \dot{u}_{\eta_1} &= f(V_{EAS}, H) \\ \dot{u}_{\eta_2} &= f(V_{EAS}, H) \\ &\dots \\ \dot{r}_{\dot{\eta}_{N_{modes}-1}} &= f(V_{EAS}, H) \\ \dot{r}_{\dot{\eta}_{N_{modes}}} &= f(V_{EAS}, H) \end{aligned} \tag{4}$$

Altogether, the 15 modes with the lowest frequency are used within the model, thus $N_{modes} = 15$. In addition to the rigid-body equations of motion, the structural dynamics equations of motion are added for each mode, again only respecting the deviations from the flight shapes:

$$\Delta\ddot{\eta}_i = -\omega_{0,i}^2 \cdot \Delta\eta_i - 2D_i\omega_0 \cdot \Delta\dot{\eta}_i + \frac{Q_i}{m_i} \tag{5}$$

As the linearised system matrix and the input matrix of the structural dynamic model (section 3.1) are available for all flight points, the generalised forces Q_i/m_i can be obtained using the derivatives with respect to the other modes' deformations and rates and the rigid-body states and inputs:

$$\begin{aligned} \frac{Q_i}{m_i} = \quad & \ddot{\eta}_{i_u}\Delta u_A + \ddot{\eta}_{i_v}\Delta v_A + \ddot{\eta}_{i_w}\Delta w_A + \ddot{\eta}_{i_p}\Delta p + \ddot{\eta}_{i_q}\Delta q + \ddot{\eta}_{i_r}\Delta r + \ddot{\eta}_{i_\xi}\Delta\xi + \ddot{\eta}_{i_{i_H}}\Delta i_H + \ddot{\eta}_{i_\zeta}\Delta\zeta + \ddot{\eta}_{i_T}\Delta T \\ & + \sum_j^{N_{modes}} \ddot{\eta}_{i_{\eta_j}}\Delta\eta_j + \sum_j^{N_{modes}} \ddot{\eta}_{i_{\dot{\eta}_j}}\Delta\dot{\eta}_j \end{aligned} \tag{6}$$

Note that these derivatives are again given for each flight shape and altitude:

$$\begin{aligned} \ddot{\eta}_{1_u} &= f(V_{EAS}, H) \\ \ddot{\eta}_{2_u} &= f(V_{EAS}, H) \\ &\dots \end{aligned} \tag{7}$$

In this modelling approach, the airspeed, in principle, affects both the quasistatic aerodynamics given for the 1g-flight shape (interpolated using V_{EAS}) and the excitation of the structural modes (use of Δu_A, Δv_A and Δw_A in equation (6)). Thus, it has to be ensured that an excursion of the airspeed does not lead to both a change of flight shape and an excitation of the modes at the same time, otherwise the effect of flexibility would be included twice. In order to prevent this from happening, a frequency-dependent separation is performed. For all interpolations in the equations (2), (4) and (7) the low-pass filtered value of the equivalent airspeed $V_{EAS,LP}$ is used instead of V_{EAS}. A cutoff frequency of $0.5\,$Hz is used. In contrast, in equation (6), the remaining high-pass portions are used to calculate Δu_A, Δv_A and Δw_A.
Furthermore, the quasistatic aerodynamic derivatives are only given for the shapes at an unaccelerated 1g-flight and already respect the trim inputs at this flight point (aileron ξ, stabiliser i_H , rudder ζ and thrust T). Hence, in order to correctly represent quasistatic flight conditions with a higher load factor, excess thrust or a different stabiliser setting, the trimmed flight conditions for the respective 1g-flight shapes are used as a reference to calculate the delta values in equation (6).

3.1 Structural Dynamic Modelling

This section describes the structural dynamics model used within the project *HAP*. Please note that this model is not directly used within this work. Instead, it was linearised at different flight points and the flexible parameters of the linear model were used for modelling the structural dynamics in the flight dynamics model described in section 3.
The finite element model (FEM) used to describe the structural dynamic characteristics is designed for aeroelastic and loads applications [24, 26, 27, 28] and is now also considered in the flight mechanical analysis. The focus on aeroelastic aspects leads to a number of requirements which differ

from a classical finite element model for stress analysis. The model should represent global elastic characteristics such as wing bending and twist, which are of major interest for loads and aeroelasticity. Local effects such as stress concentrations at sharp edges or at holes are neglected. This means that all primary structural components, such as spars, ribs and skin, should be modelled.
Because of the slender, beam-like structure of the configuration, mainly beam and bar elements are used to model the structure. The element stiffness and material characteristics are converted to a MSC.Nastran model using a combination of the parameterised model generator ModGen [29] and Microsoft Excel.
Structural masses are derived from the element dimensions combined with material thickness and density, and are complemented by the system masses. All masses are attached to the closest structural grid points as concentrated masses. Note that the structural models and mass models are treated separately because some structural members (e.g., joints, adhesives, mountings, etc.) are not included in the beam model but should be accounted for in the mass model.
The resulting structural model and the mass discretisation are shown in Figure 3. The volume of the yellow spheres is proportional to the mass they represent and the large, transparent sphere indicates the centre of gravity.

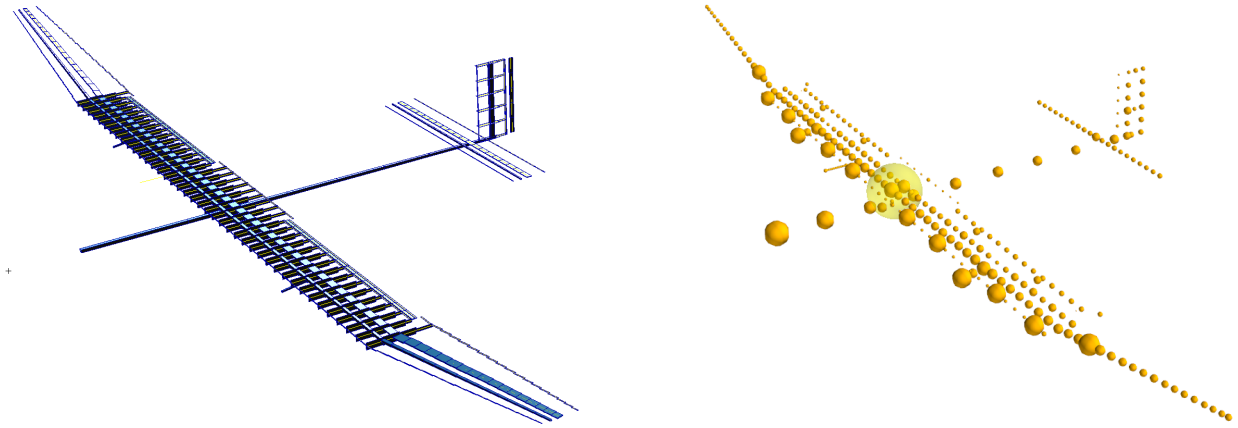

(a) MSC.Nastran beam model (b) Mass discretisation

Figure 3 – Beam model and discretisation of masses

The eigenforms and eigenfrequencies characterise the structural dynamic behavior of an aircraft and are important for aeroelastic and flight mechanical analyses. Figure 4 shows the four lowest frequency flexible mode shapes, calculated for the unconstrained aircraft in vacuum.

4. Modelling of Uncertainties

This section presents the parameters that are varied in order to model uncertainties and the process followed in order to calculate the eigenmodes of the aircraft being subject to uncertainties.

4.1 Varied Parameters

Table 1 summarises all parameters that are varied in the context of this work. In addition, it provides the variation range. These variation ranges are defined together with the experts of aerodynamics, structure and aeroelastics of the project *HAP*. They are partly based on engineering judgement, the particularities of the HAP aircraft manufacturing, and on the underlying methods used to calculate the underlying parameters.
In this work, all variations are applied to the parameters in Table 1 alone. This signifies that respective dependent parameters are not changed accordingly. For instance, a change of the mass would also have an influence on the structural dynamics and mass moments of inertia. However, these dependent parameters are not varied as a result of a mass variation.
In the following, a brief explanation of the chosen limits are given:

- Mass m: The DLR HAP aircraft is an unmanned aircraft and therefore the payload only con-

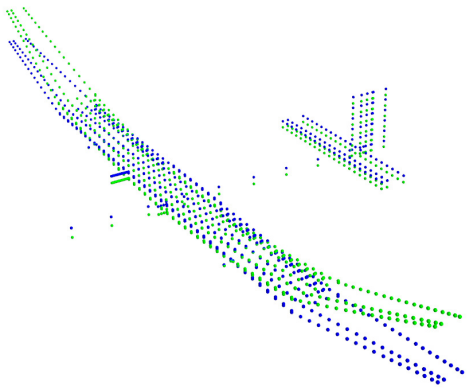

(a) Mode 1, first symmetric wing bending, $f = 0.95$ Hz

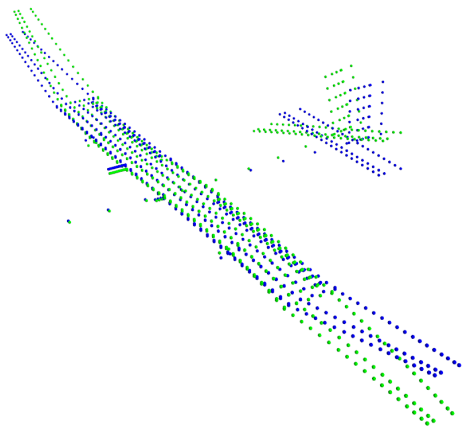

(b) Mode 2, first anti-symmetric wing bending + fuselage torsion, $f = 2.25$ Hz

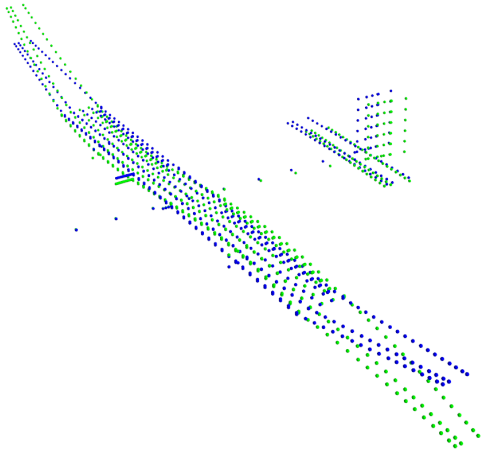

(c) Mode 3, first anti-symmetric wing bending + lateral fuselage bending, $f = 2.35$ Hz

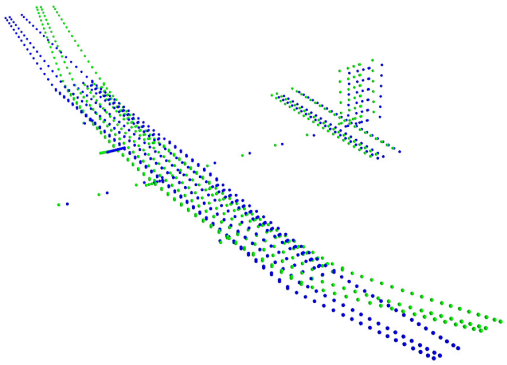

(d) Mode 4, in-plane wing bending, $f = 2.99$ Hz

Figure 4 – First flexible mode shapes

sists of the instruments. During the flight test campaign, the instruments will be omitted and not all batteries are required. Therefore, mass uncertainties, e.g., due to manufacturing variances of different parts, can easily be counteracted by excluding a battery block and/or adding supplementary masses. Therefore, the small but still conservative range of ± 5 kg is used.

- Centre of gravity (CG) coordinates x_{CG}, y_{CG} and z_{CG}: The majority of the masses is located in the wing area, as also shown by Figure 3b. As the wing is in close proximity to the CG, shifts of the latter are likely to be very small even in case of a higher deviation of the masses from the nominal configuration. The chosen ranges are conservative.

- Mass moments of inertia I_{xx}, I_{yy}, I_{zz} and I_{xz}: For I_{xx}, I_{yy} and I_{zz} ranges of $\pm 10\,\%$ are chosen, respecting both manufacturing and assembling uncertainties with respect to the mass distribution and several effects that each lead to clearly smaller variations. Potential causes for a variation of the mass moments of inertia are a variation of the total weight and deformations of the aircraft in flight which lead to a variation of the CG and the mass distribution. For I_{xz} the larger range of $\pm 20\,\%$ is chosen because the baseline value is already very small and therefore differences in the mass distribution lead to higher relative changes.

- Lift derivatives for wing-body $C_{L\alpha_{WB}}$ and horizontal tailplane $C_{L\alpha_H}$: Since the longitudinal aerodynamics are described by a two-point model the lift curve slopes are varied here rather than the pitching moment coefficients. The relatively low values of $\pm 5\,\%$ can be chosen because the effect of the very slender fuselage is negligible and the characteristics of the high-aspect-ratio

Table 1 – Varied parameters and variation range

Parameter	Variation type	Lower variation limit	Upper variation limit
m	relative	$-5\,\%$	$+5\,\%$
x_{CG}	absolute	$-10\,\text{cm}$	$+10\,\text{cm}$
y_{CG}	absolute	$-10\,\text{cm}$	$+10\,\text{cm}$
z_{CG}	absolute	$-10\,\text{cm}$	$+10\,\text{cm}$
I_{xx}	relative	$-10\,\%$	$+10\,\%$
I_{yy}	relative	$-10\,\%$	$+10\,\%$
I_{zz}	relative	$-10\,\%$	$+10\,\%$
I_{xz}	relative	$-20\,\%$	$+20\,\%$
$C_{L\alpha_{WB}}$	relative	$-5\,\%$	$+5\,\%$
$C_{L\alpha_H}$	relative	$-5\,\%$	$+5\,\%$
$C_{l\beta}$	relative	$-10\,\%$	$+10\,\%$
C_{lp}	relative	$-10\,\%$	$+10\,\%$
C_{lr}	relative	$-20\,\%$	$+20\,\%$
$C_{n\beta}$	relative	$-10\,\%$	$+10\,\%$
C_{np}	relative	$-20\,\%$	$+20\,\%$
C_{nr}	relative	$-5\,\%$	$+5\,\%$

lifting surfaces can be calculated with a comparably high accuracy even using Vortex Lattice Methods.

- Rolling moment derivatives $C_{l\beta}$, C_{lp} and C_{lr}: Since the aerodynamic effect of the fuselage is, as already mentioned, very small, $C_{l\beta}$ mainly depends on the wing and vertical tailplane. C_{lp}, mainly depending on the high-aspect-ratio wing's lift characteristics, can also be calculated with reasonable accuracy. For both, the moderate uncertainty range of $\pm 10\,\%$ is thus chosen. C_{lr}, on the other hand, involves yawing and rolling motion and is therefore more prone to uncertainties. In addition, the baseline value is small. Consequently, $\pm 20\,\%$ is chosen.
- Yawing moment derivatives $C_{n\beta}$, C_{np} and C_{nr}: Similarly to the rolling moment derivatives, $C_{n\beta}$ is barely affected by the fuselage for the given aircraft and thus the moderate uncertainty range $\pm 10\,\%$ is chosen. Similarly to C_{lr}, C_{np} involves yawing and rolling motion and its calculation is therefore subject to a higher uncertainty. C_{nr} nearly exclusively depends on the vertical tailplane and can thus be assumed to be relatively accurate. Therefore, a range of $\pm 5\,\%$ is chosen.

4.2 Calculation Process

This section describes the calculation process followed to obtain the resulting eigenmodes for the DLR HAP aircraft subject to uncertainties. As already described in section 3 the flexible model includes the reference conditions for the trimmed 1g-flight shapes for which the derivatives are given. The flexible modes are excited by all parameters that deviate from these reference conditions. In order to ensure that variations of the aerodynamic parameters are treated as uncertainties of the aerodynamic properties at the given flight shapes, the underlying 1g-flight shapes need to be updated in the model respecting the uncertainties. Figure 5 shows the associated flow chart.

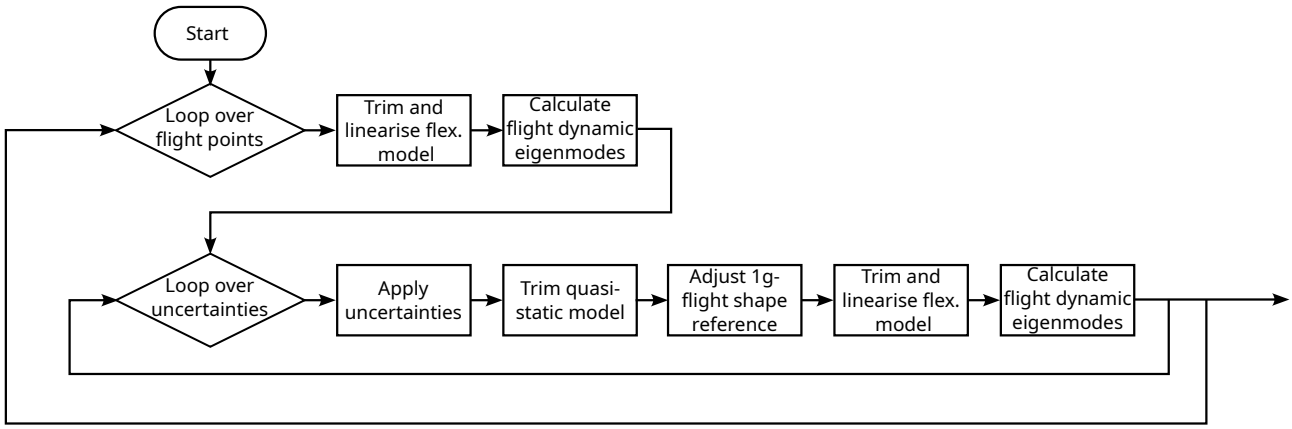

Figure 5 – Flow chart of the calculation process used to obtain the eigenmodes

5. Eigenmode Analysis

This section presents the DLR HAP aircraft's eigenmodes. First of all, the eigenmodes of the baseline configuration are shown. Second, a sequential variation of parameters is performed, showing the sensitivity of the eigenmodes to the parameter variations. Finally, a simultaneous variation is performed that gives an idea of how strong the deviation from the baseline can be if all uncertainties are considered.

5.1 Baseline Configuration

In [19], an extensive flight mechanics analysis has been presented for the DLR HAP aircraft. However, there have been various updates as well of the aircraft and of the flight dynamics model used. Some of the most important updates are:

- The structural dynamics are now included in the flight dynamics model.
- The mass distribution inside the wing has been changed leading to differences, particularly with respect to wing deformation.
- The never-exceed speed was decreased from 15.5 m/s to 14.5 m/s to cope with sizing loads issues.

For these reasons, an update of the eigenmodes of the nominal DLR HAP aircraft will be presented here before showing the sensitivity analysis. Figure 6 provides the roots of the current DLR HAP aircraft.

Figure 6a shows all roots of the nominal configuration, including rigid-body eigenmodes and the flexible modes. These are given for the complete envelope of the aircraft. The different altitudes are emphasised by a different colour, and the velocities are represented by different markers. The design speeds shown in Figure 2 have larger markers, while intermediate velocities have smaller dot markers. As shown, the roots are widespread over the complete pole plot.

Figure 6b provides a zoom of the pole plot, revealing the strongly decaying aperiodic roll mode and the short period. As discussed in [19], the DLR HAP aircraft does not have a short period mode in the classical sense. Instead, due to the low mass of the aircraft, the respective mode also involves a change of altitude to a large extent. Figure 6b furthermore shows the first wing bending mode, having a frequency of around 1 Hz, which is in a similar order of magnitude as the short period mode. At high altitudes, short period and first wing bending do not interfere. While the first is weakly damped, the latter is aperiodic. However, at lower altitudes, the short period becomes stronger damped. At FL 0 and FL 200, it is characterised by two stable fast decaying modes. The first wing bending mode, on the other hand, becomes oscillatory at intermediate altitudes and low speeds.

As shown, at FL 200 and at high speeds (violet markers and close to V_{NE}), one of the previously aperiodic modes of the short period and one of the first wing bending modes start to couple and form a strongly damped oscillatory mode. However, time history analyses and pilot-in-the-loop studies have shown that this mode does not have a recognisable effect on the aircraft's flight behaviour.

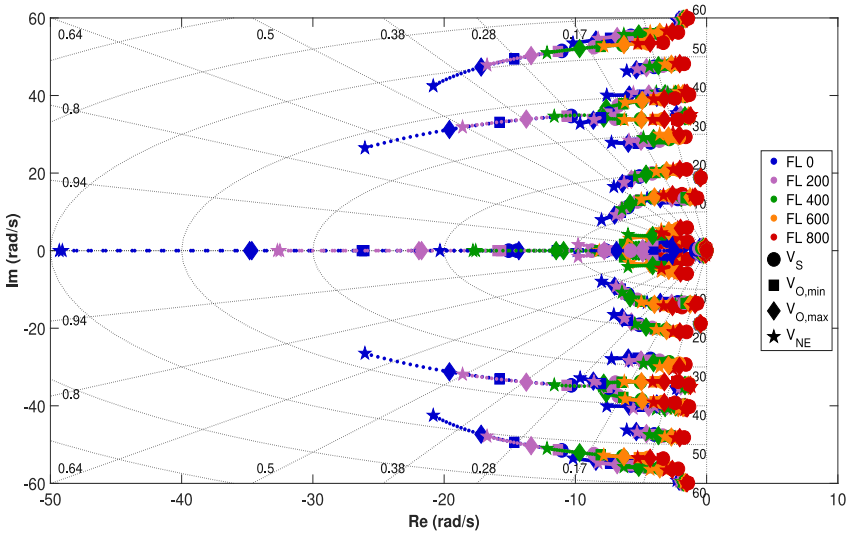

(a) Overview

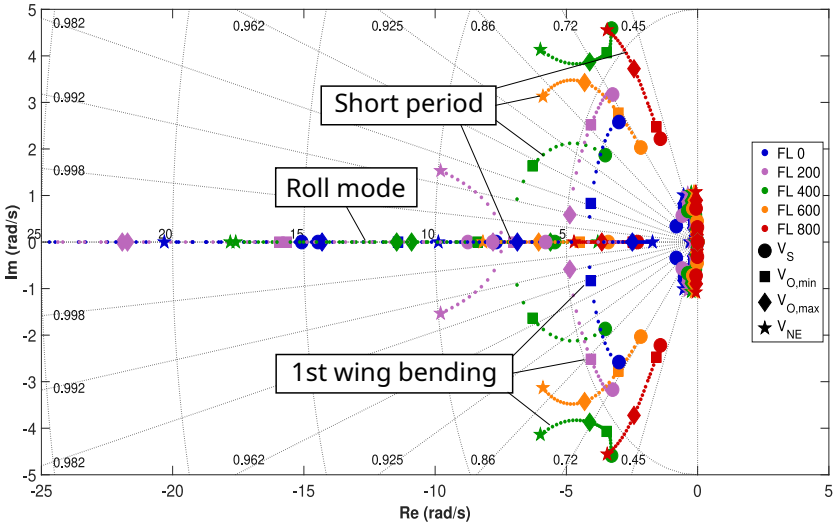

(b) With zoom

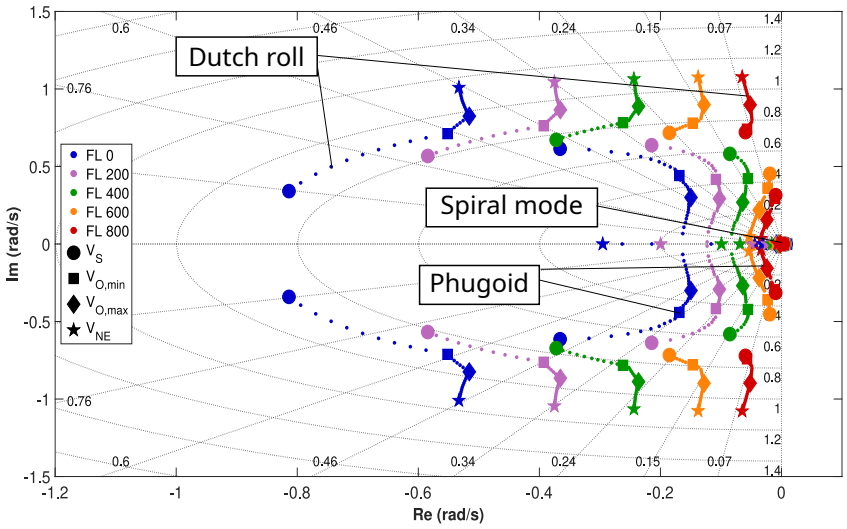

(c) With increased zoom

Figure 6 – Roots of the nominal configuration

Figure 6c provides an increased zoom of the pole plot, showing the Dutch roll, the phugoid and the spiral mode. The Dutch roll's characteristics significantly depend on the altitude. At low altitudes, this mode is very strongly damped and has a moderate frequency. At V_S the respective roots are already close to the real axis. At high altitudes, on the other hand, this mode is weakly damped and has a low frequency.
Similarly to the short period mode, the phugoid mode of the DLR HAP aircraft differs significantly from the classical phugoid mode. It is strongly damped and has a high frequency, compared to the more typical phugoid. This behaviour results both from the low weight of the aircraft and its low velocity, leading to a lower amount of energy in the phugoid motion. It can be seen that this mode becomes aperiodic at all altitudes at velocities close to V_{NE}. Nevertheless, none of the aperiodic poles become unstable at any flight point.
Finally, Figure 6c shows the spiral mode. It is an aperiodic mode with a real part near zero. At all velocities this pole becomes unstable at velocities close to V_S. However, the lowest time to double amplitude of the spiral in the complete envelope is around 23 s. According to typical handling qualities criteria for manned aircraft, as can be found for instance in MIL-STD-1797A [30], this value still represents satisfactory handling from a pilot's point of view. Indeed, the HAP aircraft is not a manned aircraft and will be piloted remotely. However, in this case it can be assumed that the assessment is transferable because it does not involve the pilot's perception: it rather states that, with such a long time to double amplitude, the pilot will counteract the spiral mode inadvertently while commanding other manoeuvres. This is also applicable for remote flight.
In summary, the nominal flying qualities of the DLR HAP aircraft are acceptable.

5.2 Sequential Parameter Variation – Sensitivity Analysis

This section deals with a sensitivity analysis of the aircraft's eigenmodes with respect to different parameters. Contrary to performing a worst-case analysis respecting all parameter variations, such an approach yields important qualitative information that can be used to decide which parameters should be calculated with more accurate methods within the design process.
The sensitivity analysis is performed in such a way that all parameters summarised in Table 1 are varied consecutively, i.e., one parameter at a time. The parameters are varied from the nominal value until the minimum, respectively maximum values, with two equidistant steps each.
Figure 7 shows the influence of longitudinal parameter variations on the phugoid's damping and natural frequency at FL 0 and V_S (7a) and at FL 800 and $V_{O,max}$ (7b).
First of all, it is notable that variations have a stronger effect at the lower flight point. The CG in x coordinate has a relatively strong effect at both flight points, while an increase, i.e., a shift of the CG aft, decreases damping and increases the frequency. A variation of the CG in z-direction (an increase signifies a shift to the top) has a similar but weaker effect. It is interesting to note that the mass, having a significant influence especially on the damping, has an opposed effect between both flight points. While an increase leads to an increased damping at the lower flight point, it reduces damping at the higher altitude. It has the same effect with respect to frequency. The effect of the wing-body lift curve slope $C_{L\alpha_{WB}}$, however, is opposed with respect to damping and frequency. Nevertheless, its influence is rather small at the higher flight point.
Figure 8 shows the influence of longitudinal parameter variations on the short period mode. At FL 0 and V_S, where this mode is aperiodic, but still mostly unaffected by the first wing bending, the first aperiodic mode (8a) and the second aperiodic mode (8b) are shown. Furthermore, Figure 8c shows the parameter variation effect on the oscillatory mode at FL 800 and V_{NE}.
Comparing the aperiodic modes at the flight point, it can be observed that most parameter variations have an opposing effect on both modes, both in magnitude and in direction. The effects suggest that the first aperiodic mode involves a pitching movement to a large extent. This is reflected by the strong influences of the CG in x-direction, the mass moment of inertia about the pitch axis I_{yy}, and $C_{L\alpha_H}$. Compared to $C_{L\alpha_{WB}}$ $C_{L\alpha_H}$ primarily has influences during a pitching movement due to its large lever arm.
The second aperiodic mode, on the other hand, involves altitude change to a larger extent, which is reflected by the stronger influences of the mass and $C_{L\alpha_{WB}}$.

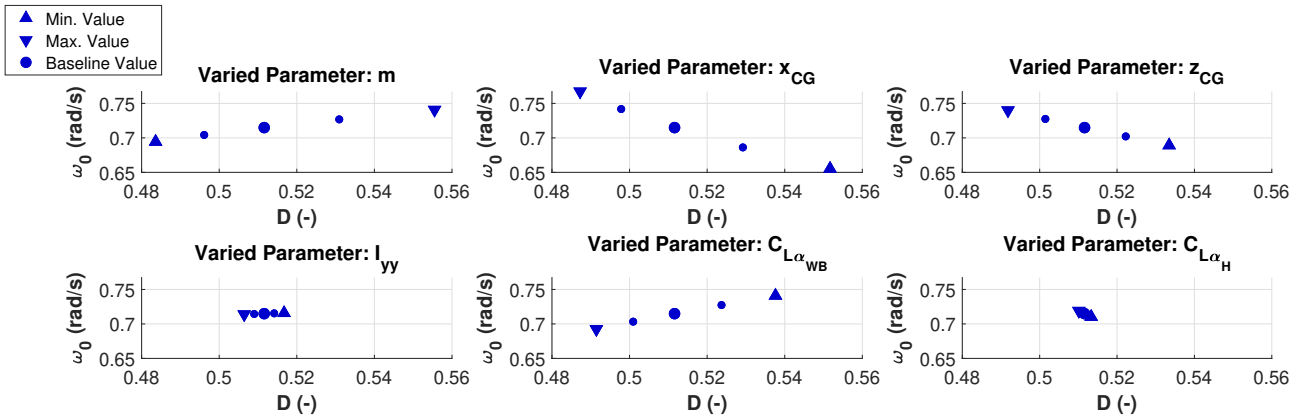

(a) Oscillatory root, flight point at FL 0 and V_S

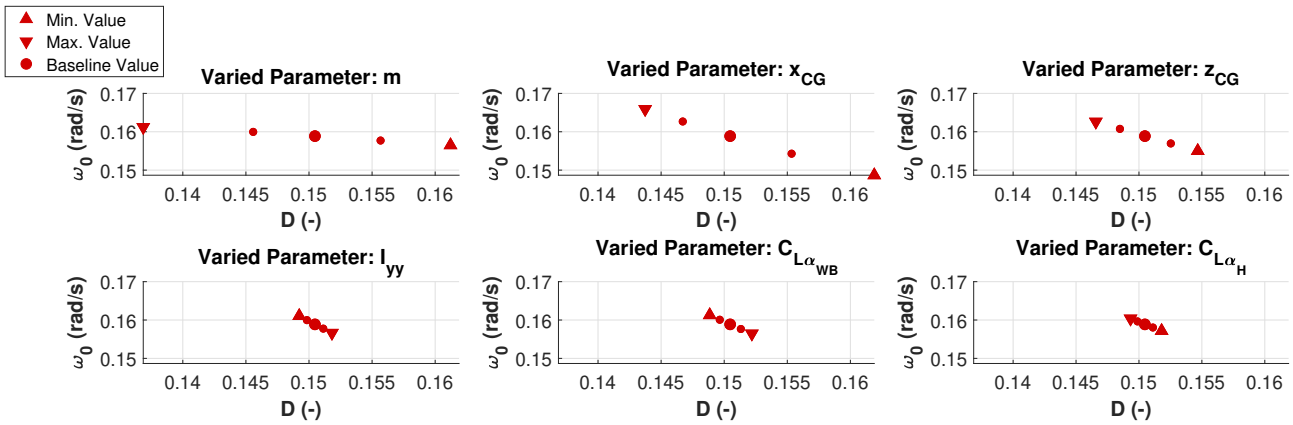

(b) Oscillatory root, flight point at FL 800 and $V_{O,max}$

Figure 7 – Sensitivity of phugoid to variation of longitudinal parameters

At FL 800 and V_{NE} the aircraft has an oscillatory mode, which is more similar to a classical short period mode. Accordingly, the CG-position in x-direction has a strong effect, whereas a shift aft decreases damping and increases the frequency. Altogether, for the given ranges, the parameter variation effects are moderate at this flight point.

Figure 9 shows the influence of lateral-directional parameter variations on the Dutch roll's damping and natural frequency at FL 0 and V_S (9a) and at FL 800 and V_{NE} (9b).

As shown, the effects are, from a qualitative point of view, similar for most parameter variations and as expected. An increase of the mass moment of inertia about the z-axis decreases damping and frequency, $C_{l\beta}$ decreases damping and C_{nr} increases damping.

However, it is noteworthy that the coupling derivatives C_{lr} and C_{np} play a much larger role at the lower flight point and a variation of these parameters has a strong effect. At the higher flight point, the damping derivatives C_{lp} and C_{nr} become more important.

Finally, it should be noted that a variation of I_{xx}, I_{xz} and the CG in y-position have, at least in the given range, hardly any effect.

Figure 10 shows the effects of lateral-directional parameter variations on the aperiodic roll mode at FL 0 and V_S. It can be stated that the results are not surprising for the roll mode of a very-high-aspect-ratio-wing aircraft. The mass moment of inertia about the x-axis I_{xx} and the roll damping C_{lp} are the main drivers here. It is, however, interesting to note that the variations lead to large changes of the root locations.

Finally, Figure 11 presents the variation influences on the spiral mode at FL 0 and V_S.

Most of the effects are as expected. This includes $C_{l\beta}$ and C_{nr}, which both stabilise this mode. $C_{n\beta}$ destabilises the spiral mode at this flight point. Nevertheless, C_{lr} has the strongest impact on the spiral mode, where an increase leads to a destabilisation. Indeed, with a variation range of $\pm 20\,\%$, this parameter was varied stronger than most other parameters. However, even a reduction by 10 % already yields a stable spiral. This shows that this parameter, which was deemed to be more difficult

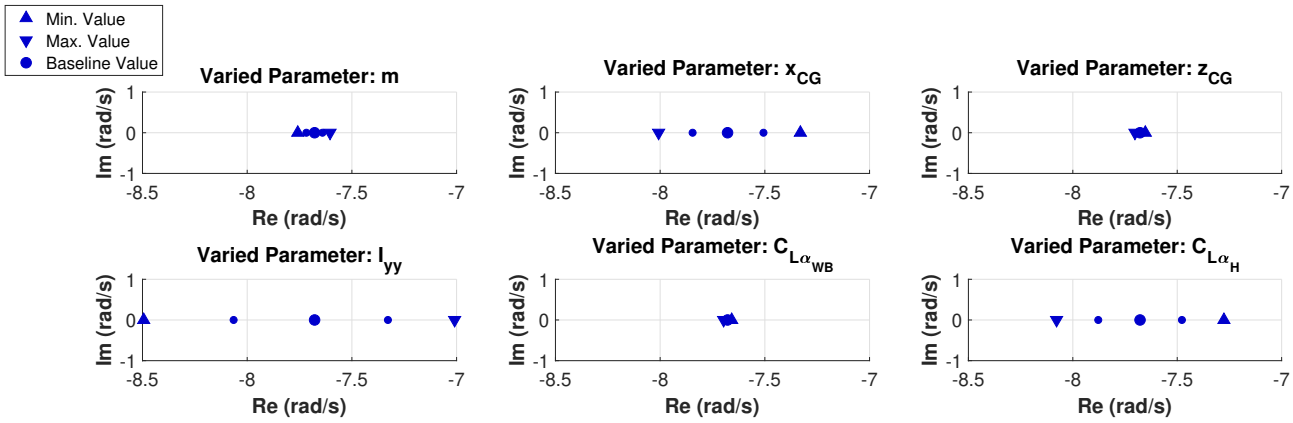

(a) First aperiodic root, flight point at FL 0 and V_S

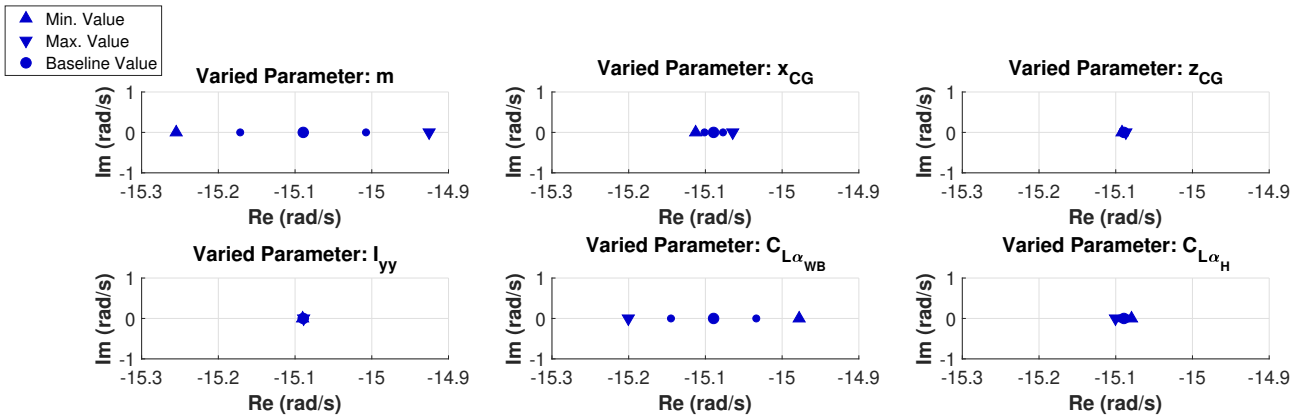

(b) Second aperiodic root, flight point at FL 0 and V_S

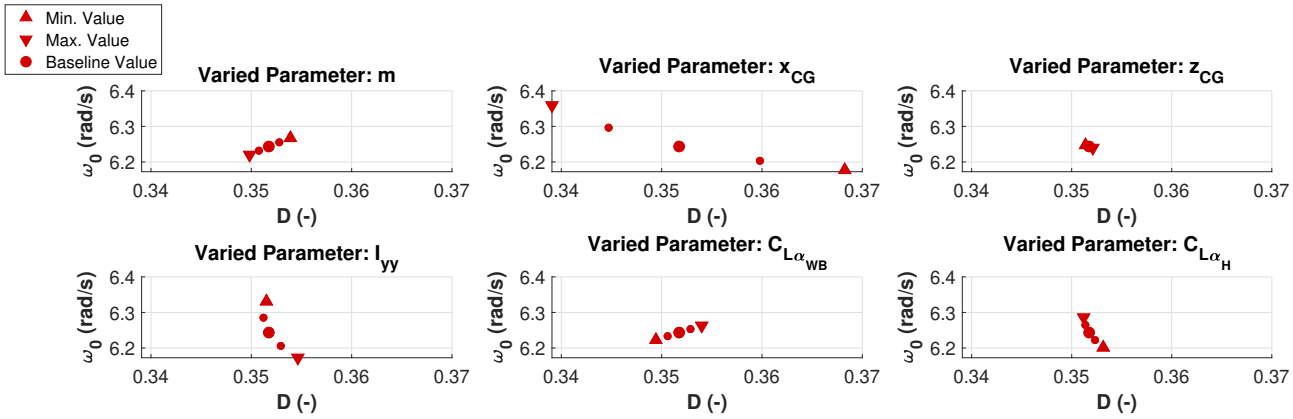

(c) Oscillatory root, flight point at FL 800 and $V_{O,max}$

Figure 8 – Sensitivity of short period to variation of longitudinal parameters

to calculate with a certain accuracy, is worth investigating in more detail.

5.3 Simultaneous Parameter Variation

After the previous qualitative analysis, which showed the sensitivity of different eigenmodes to parameter variations, this section deals with the question to which extent a combination of random parameter variations inside the given ranges leads to an excursion of the nominal flying qualities. For this reason, all parameters are varied simultaneously.

It should be noted that this approach does not replace the common worst-case analysis, in which the parameter variations are chosen as such that they have the worst possible impact as described, e.g., in [23]. However, it gives an impression of the possible effects of combined parameter variations. Furthermore, it also shows how likely significant deviations from the flying qualities of the baseline configurations are.

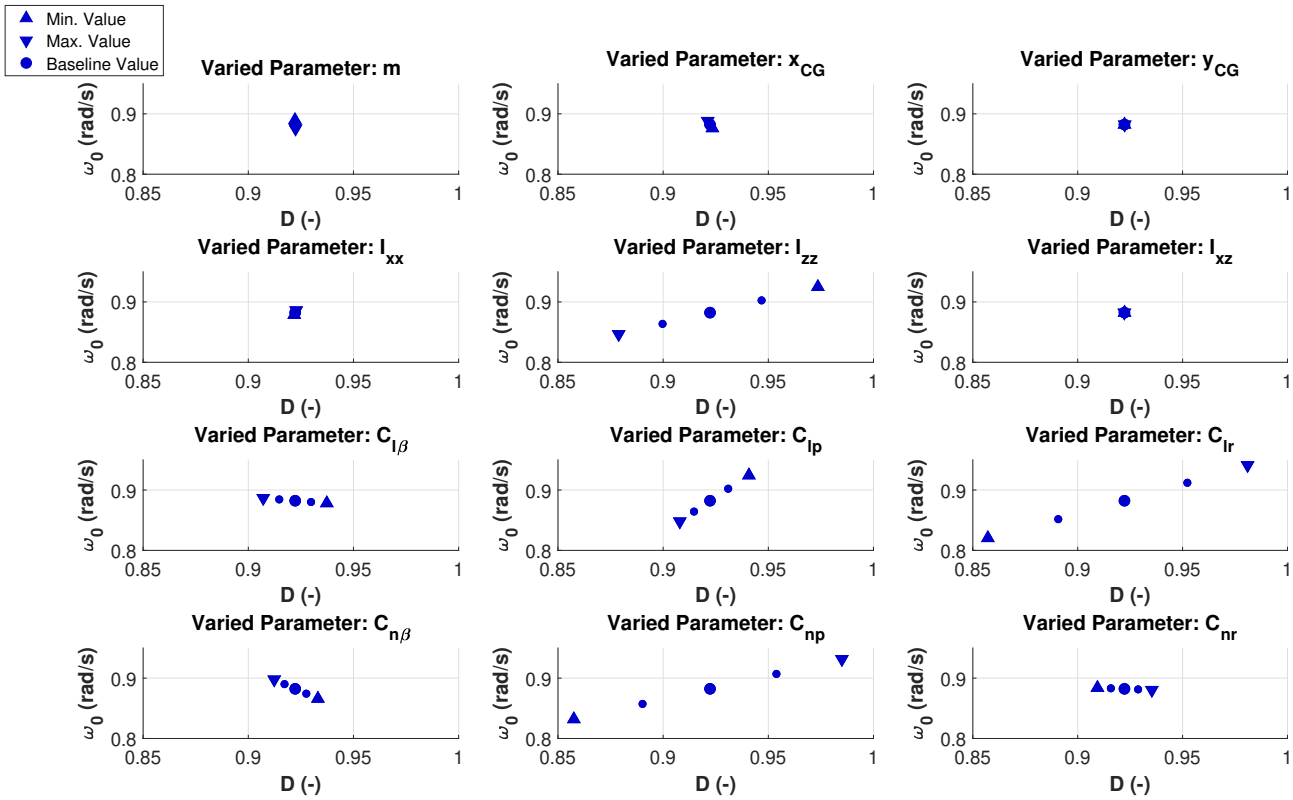

(a) Oscillatory root, flight point at FL 0 and V_S

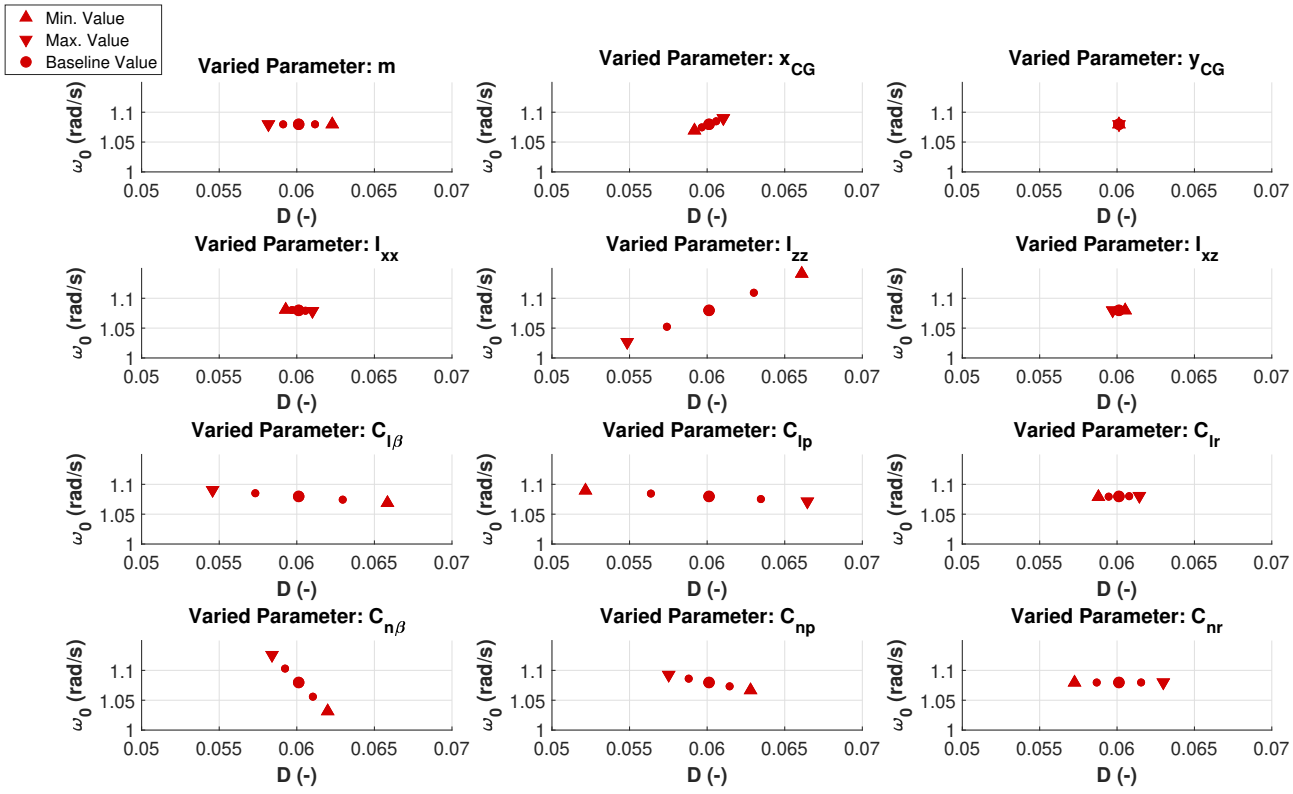

(b) Oscillatory root, flight point at FL 800 and V_{NE}

Figure 9 – Sensitivity of Dutch roll to variation of lateral-directional parameters

For this purpose, at each flight point (combination of characteristic airspeed and altitude) 50 different cases are calculated with simultaneous normally distributed random parameter variations within the ranges summarised in Table 1. The normal distribution is defined in such a way that the parameter variation limits provided in Table 1 represent the 3σ-limits. Figure 12 shows the results.

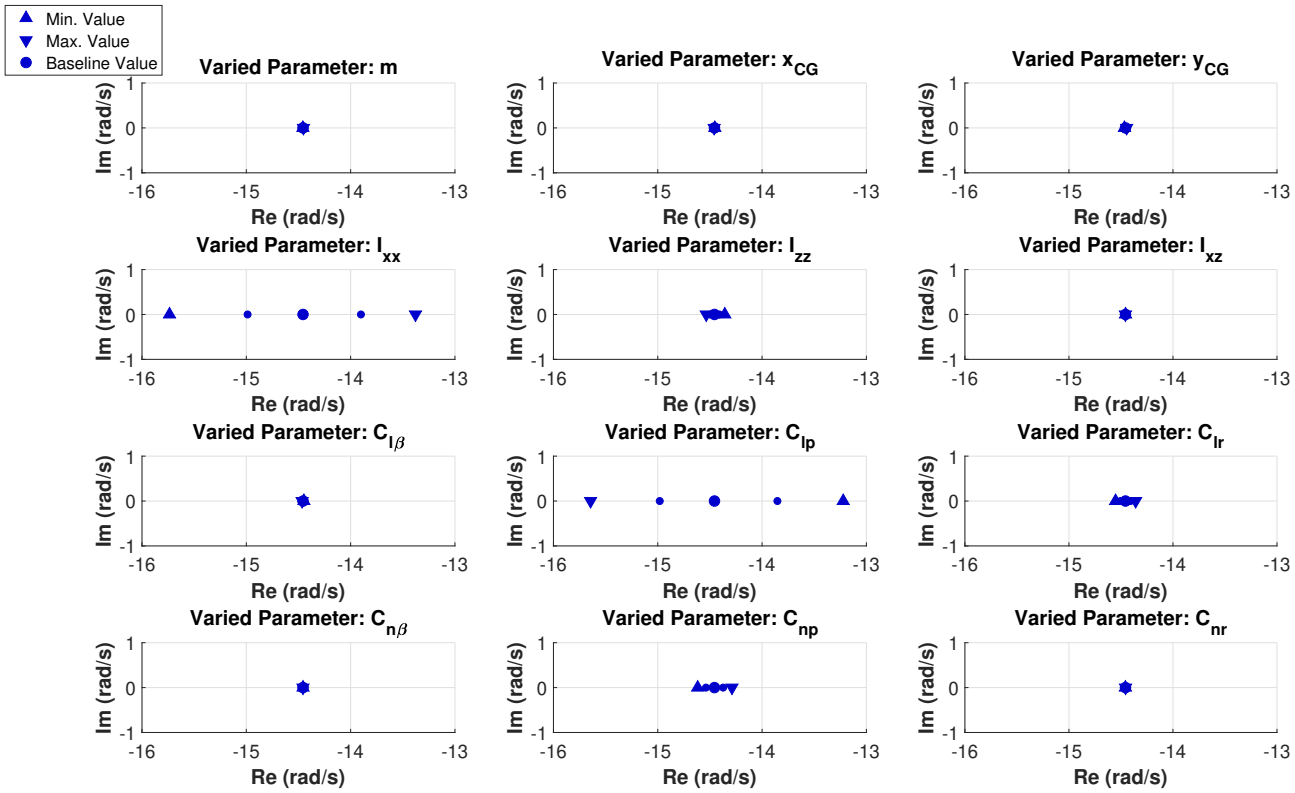

Figure 10 – Sensitivity of aperiodic roll mode to variation of lateral-directional parameters at FL 0 and V_S

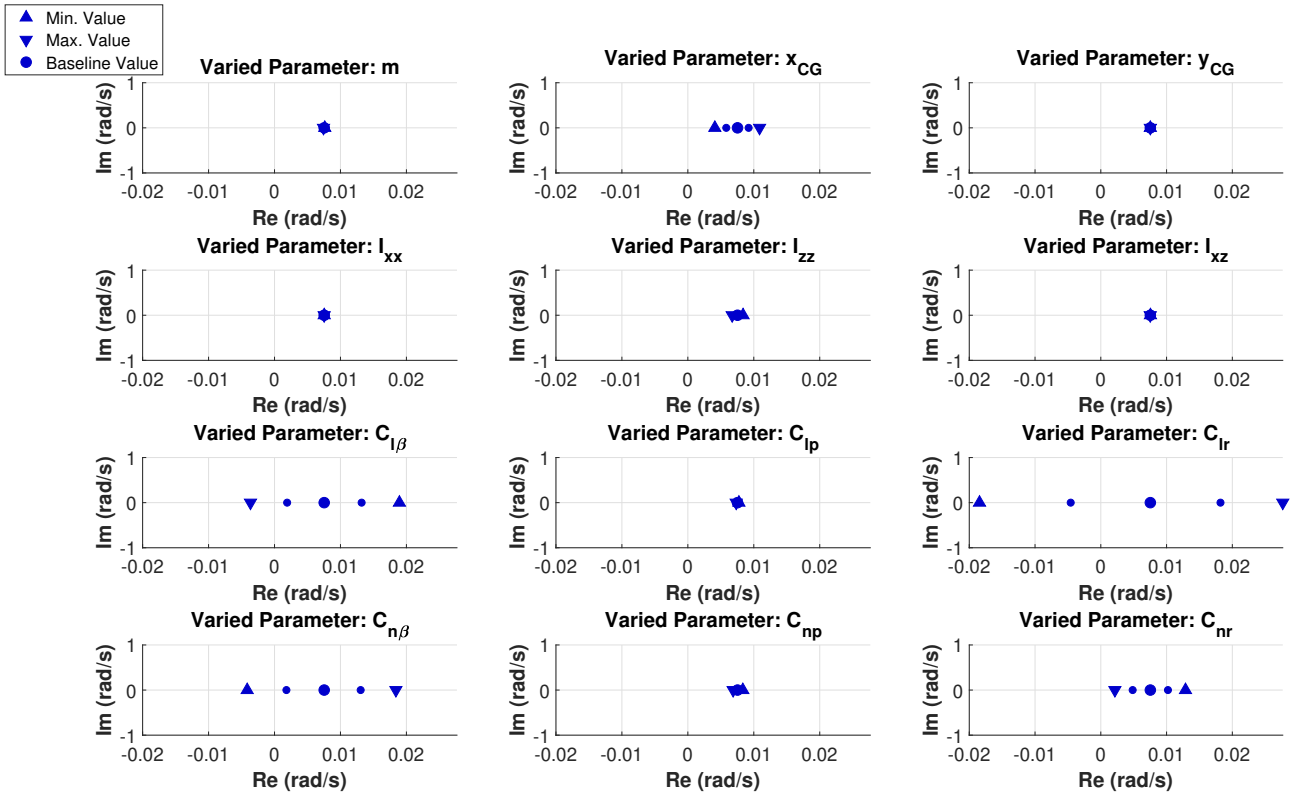

Figure 11 – Sensitivity of aperiodic spiral mode to variation of lateral-directional parameters at FL 0 and V_S

At this point, the complete pole plot as in Figure 6a is omitted and the zoomed plots are directly shown. Figure 12a presents the zoomed pole plot, showing the roll mode, the short period, the first

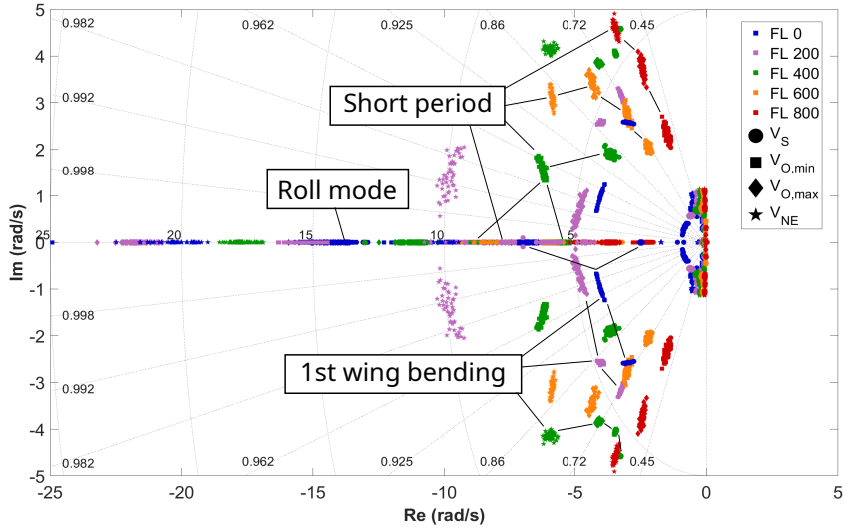

(a) With zoom

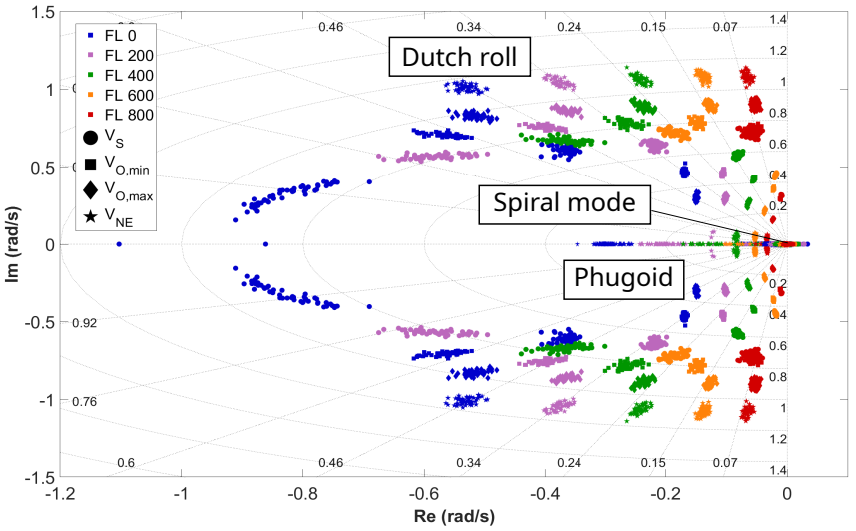

(b) With increased zoom

Figure 12 – Roots of the configuration subject to simultaneous parameter variations

wing bending modes and the oscillatory mode evolving out of the short period and the first wing bending. It can be seen that the roots resulting from the uncertainties centre around the roots of the nominal configuration. In most cases, the deviations from the latter are only moderate. The closer the nominal root is to the real axis, or if it is even an aperiodic root, the stronger the possible deviations tend to get. However, in none of the cases the uncertainties lead to unsatisfactory roots. Instead, the variations have a similar effect as a change of the velocity of the flight point (compare Figure 6b).
Figure 12b shows an increased zoom and thereby depicts the Dutch roll, spiral and phugoid roots. For the Dutch roll at low altitudes, the combined variations lead to relatively strong deviations from the nominal case. Nevertheless, the latter is strongly damped, thus none of the cases are critical. At higher altitudes, where the Dutch roll is less damped, the variations only lead to small deviations.
In case of the phugoid mode, the inclusion of uncertainties is not crucial either. Only at V_{NE}, where the roots are on the real axis, the locations of the roots deviate strongly from the nominal case. However, in none of the cases, any of the associated modes becomes unstable (this cannot be verified in the Figure 12b but it was checked within the investigations). At this point it must be noted that drag parameters which have significant influences on the phugoid were not varied within this work.
Finally, the introduction of uncertainties has an impact on the spiral mode. In the worst case consid-

ered here, it results in a time to double amplitude of the spiral mode of 21 s, as opposed to 23 s in the nominal case. This is still a sufficiently high value, leading to satisfactory handling qualities according to [30].
Altogether, in the simultaneous parameter variation investigations performed here, no critical case is identified.

6. Conclusion

The aim of this paper was to perform a flight mechanical analysis of the DLR HAP aircraft under uncertainty considerations. For this purpose, different parameters were identified and, based on the methods used to calculate these parameters within the design process and on engineering judgement, associated expected uncertainties were defined. Consecutively, a comprehensive eigenmode analysis was performed.
In a first step, the eigenmodes of the nominal aircraft were presented for the complete envelope using a flight dynamic model that incorporates quasistatic flexible effects and the structural dynamics. As shown, the eigenmodes were widespread over the pole plot. At intermediate altitudes the short period interacts with the first wing bending mode, which is in a similar frequency range. The phugoid mode has a comparatively low frequency and the Dutch roll is highly damped at low altitudes and weakly damped at high altitudes. The spiral mode is unstable at all altitudes at V_S, while the minimum time to double amplitude, thus in the worst case, is around 23 s. Altogether, the eigenmodes of the nominal aircraft are acceptable.
In a second step, all chosen parameters were varied consecutively within the afore-defined limits to show the sensitivity of these modes with respect to the uncertainties. Here, only one parameter is varied at a time while all the other parameters are kept at their baseline values. Model uncertainties proved to have a larger effect at lower altitudes and for eigenmodes that are already close to the real axis. In case of the phugoid mode, a variation of the mass and the main wing lift curve slope have an opposing effect at low altitudes and low airspeeds compared to high altitudes and high airspeeds. For the Dutch roll at low altitudes the coupling derivatives C_{lr} and C_{np} have a major effect on this mode. At higher altitudes, however, this mode behaves more like a classical Dutch roll mode. Here, it is more influenced by roll damping C_{lp}, weathercock stability $C_{n\beta}$ and static roll stability $C_{l\beta}$. For the short period mode, the sensitivity analysis was performed for a flight point where this mode has two aperiodic roots. Both roots showed opposing sensitivities indicating that one mode primarily involves pitching movements while the other one involves altitude change.
Finally, all parameters were varied randomly at the same time. For each altitude and the characteristic altitudes in the complete envelope, 50 different uncertainty combinations were generated. In this investigation, no critical case was identified, suggesting that the final manufactured and assembled DLR HAP aircraft, subject to all uncertainties, will have acceptable flight characteristics.
The simultaneous parameter variation performed in this work demonstrates how a combination of all uncertainties may lead to a deviation of the eigenmodes from the baseline configuration. However, it does not guarantee that no critical combinations exist. In addition, only 50 combinations were investigated per flight point. In order to clear the aircraft for flight testing, a worst-case analysis is necessary and will be performed in future work. Nevertheless, the simultaneous parameter variation already shows that the probability of adverse combinations is unlikely.
Finally, the results presented in this paper strongly depend on the chosen parameter variation ranges and are only valid if the latter are realistic. The definition of such uncertainties is not an easy task, especially for prototype aircraft, as, if at all, only few experience is available. However, for this reason, the uncertainties were chosen conservatively. Therefore, it is to be expected that the actual uncertainties do not exceed the ranges chosen here and the results are significant.

7. Future Work

The simultaneous parameter variation performed in this work merely serves as an outlook for future work. As already described, for a final clearance of the aircraft for flight testing, a worst-case scenario needs to be performed that demonstrates that all uncertainties combined actually do not lead to critical cases. Therefore, the next step will be to perform such a worst-case analysis using anti-optimisation.

Acknowledgements

The authors would like to thank the colleagues involved in the project *HAP*, particularly those who are part of the flight physics team and thereby contributed in setting up the flight dynamics model used in this work.

Contact Author Email Address

yasim.hasan@dlr.de

Copyright Statement

The authors confirm that they, and/or their company or organization, hold copyright on all of the original material included in this paper. The authors also confirm that they have obtained permission, from the copyright holder of any third party material included in this paper, to publish it as part of their paper. The authors confirm that they give permission, or have obtained permission from the copyright holder of this paper, for the publication and distribution of this paper as part of the ICAS proceedings or as individual off-prints from the proceedings.

References

[1] Joint Authorities for Rulemaking of Unmanned Systems. *JARUS guidelines on Specific Operations Risk Assessment (SORA), Edition 2.0, Final Release*, 30th January 2019

[2] European Union Aviation Safety Agency, *Acceptable Means of Compliance (AMC) and Guidance Material (GM) to Commission Implementing Regulation (EU) 2019/947, Issue 1, Annex I to ED Decision 2019/021/R*, 9th October 2019

[3] Runge, H., Rack, W., Ruiz-Leon, A. and Hepperle, M. A Solar Powered HALE-UAV for Arctic Research. *1st CEAS European Air and Space Conference*, Berlin, Germany, September 2007

[4] Mohammed, A., Mehmood, A., Pavlidou, F.-N. and Mohorcic, M. The Role of High-Altitude Platforms (HAPs) in the Global Wireless Connectivity. *Proceedings of the IEEE*, Vol. 99, pp. 1939-1953,doi: 10.1109/JPROC.2011.2159690, November 2011

[5] D'Oliveira, F., Melo, F. and Devezas, T. High-Altitude Platforms - Present Situation and Technology Trends. *Journal of Aerospace Technology and Management*, Vol. 8, pp. 249-262 doi: 10.5028/jatm.v8i3.699, August 2016

[6] National Aeronautics and Space Administration, Dryden Flight Research Center. Solar-Powered Research and Dryden. *NASA Facts: S-1998-10-0054 DFRC*, available online at https://www.nasa.gov/centers/dryden/pdf/120308main_FS-054-DFRC.pdf, 1998

[7] National Aeronautics and Space Administration. Environmental Research Aircraft and Sensor Technology (ERAST). *NASA Armstrong Fact Sheet: FS-020-DFRC*, available online at https://www.nasa.gov/centers/armstrong/news/FactSheets/FS-020-DFRC.html, 28th February 2014)

[8] Ross, H. Fly Around the World with a Solar Powered Airplane. *Technical Soaring, An International Journal*, Vol. 32, No. 4 doi: 10.2514/6.2008-8954, September 2008

[9] Nunez, C. Solar Impulse 2 Completes Trip Around World, Demonstrates Clean Energy and Aviation. *National Geographic*, Available online at https://www.nationalgeographic.com/news/2016/07/solar-impulse-completes-trip-around-world-abu-dhabi-solar-power-airplane/, 25th July 2016

[10] Stevens, P. Zephyr: Pioneering the Stratosphere, ZP-PN-0039v2.0. *Exploring an Unmanned Future Conference, Australian Association for Unmanned Systems*, Melbourne and Avalon, Presentation, available online at https://aaus.org.au/wp-content/uploads/2019/03/Paul-Stevens-Airbus-at-AAUS-Exploring-an-Unmanned-Future-Conference-20190225.pdf, 25th February 2019

[11] Airbus Defence and Space. Airbus Zephyr, Solar High Altitude Pseudo-Satellite flies for longer than any other aircraft during its successful maiden flight. *Press Release*, available at https://www.airbus.com/en/newsroom/press-releases/2018-08-airbus-zephyr-solar-high-altitude-pseudo-satellite-flies-for-longer, 8th August 2018

[12] Malewar, A. Airbus's solar-powered Zephyr UAS crashes after a 64-day flight. *Inceptive Mind*, Available online at https://www.inceptivemind.com/airbus-solar-powered-zephyr-uav-crashes-64-day-flight/25969/, 25th August 2022

[13] BAE Systems. *Ground-breaking solar powered unmanned aircraft makes first flight*, Available online at https://www.baesystems.com/en/article/ground-breaking-solar-powered-unmanned-aircraft-makes-first-flight, Retrieved July 2022

[14] UAVOS. UAVOS Flight Tests ApusDuo Stratospheric Platform, Available online at https://www.uavos.com/uavos-flight-tests-apusduo-stratospheric-platform/, Retrieved July 2022

[15] Noll, T.E., Brown, J.B., Perez-Davis,W.E., Ishmael, S.D., Tiffany, G.C and Gaier,M. Investigation of the Helios Prototype Aircraft Mishap. *NASA - Helios Mishap Investigation Board*, 16th January 2004

[16] National Transportation Safety Board. *Aviation Accident Report - Accident DCA15CA117, Titan Solara 50, N950TA*, 1st May 2015

[17] National Transportation Safety Board. *Aviation Accident Report - Accident DCA16CA197, Facebook Aquila, N565AQ*, 28th June 2016

[18] Australian Transport Safety Bureau. *Aviation safety investigations & reports - AO-2019-056, Airbus Zephyr*, 28th September 2019

[19] Hasan, Y. J., Roeser, M. S., Hepperle, M., Niemann, S., Voß, A., Handojo, V. and Weiser, C. Flight mechanical analysis of a solar-powered high-altitude platform. *CEAS Aeronautical Journal*, Vol. 14, pp. 201–223, doi: 10.1007/s13272-022-00621-2, November 2022

[20] Hasan, Y. J., Roeser, M. S. and Voigt, A. Evaluation of the controllability of a remotely piloted high-altitude platform in atmospheric disturbances based on pilot-in-the-loop simulations, *CEAS Aeronautical Journal*, Vol. 14, pp. 225–242, doi: 10.1007/s13272-022-00626-x, November 2022

[21] Hasan, Y. J., Fezans, N. and Voß, A. Landing Simulation of a High-Altitude Platform with Skid-Type Landing Gear - Flight Procedure, Controller, and Loads. *33rd Congress of the International Council of the Aeronautical Sciences*, Stockholm, Sweden, September 2022

[22] Hasan, Y. J. Evaluation of Landing Procedures for a High-Altitude Platform with Skid-Type Landing Gear Based on Pilot-in-the-Loop Simulations. *Deutscher Luft- und Raumfahrtkongress (German Aerospace Congress)*, Stuttgart, Germany, September 2023

[23] Fielding, C., Varga, A., Bennani, S. and Selier, M. *Advanced Techniques for Clearance of Flight Control Laws*, Springer, June 2002

[24] Voß, A., Handojo, V., Weiser, C. and Niemann, S. Preparation of loads and aeroelastic analyses of a high altitude, long endurance, solar electric aircraft. *AEC2020 Aerospace Europe Conference*,https://elib.dlr.de/133496/, Bordeaux, France, 2020

[25] Waszak, M. R. and Schmidt, D. K. Flight dynamics of aeroelastic vehicles. *Journal of Aircraft*, Vol. 6, No. 25, doi: 10.2514/3.45623, June 1988

[26] Voß, A., Handojo, V., Weiser, C. and Niemann, S. Results from Loads and Aeroelastic Analyses of a High Altitude, Long Endurance, Solar Electric Aircraft. *Journal of Aeroelasticity and Structural Dynamics*, Vol. 9, No. 1, pp. 1-22, doi: 10.3293/asdj.2021.58, January 2022

[27] Voß, A., Koch, C., Niemann, S., Mantei, M., Handojo, V. and Weiser, C. Transition From Preliminary to Detailed Design of a Highly Elastic Solar Electric Aircraft. *International Forum on Aeroelasticity and Structural Dynamics*, https://elib.dlr.de/186492/, Madrid, Spain, 2022,

[28] Weiser, C., Schulz, S., Voß, A. and Ossmann, D. Attitude Control for High Altitude Long Endurance Aircraft Considering Structural Load Limits. *AIAA SciTech 2023 Forum*, doi: 10.2514/6.2023-0106, National Harbor, Maryland, 2023

[29] Klimmek, T. Parameterization of topology and geometry for the multidisciplinary optimization of wing structures. *CEAS 2009 - European Air and Space Conference*, Manchester, United Kingdom, 2009

[30] Department of Defense, USA, MIL-STD-1797A. *Military Standard, Flying Qualities of Piloted Aircraft*, July, 2001